# Raman scattering investigation of $Y_{1-x}Ca_xTiO_3$

Takao Tsurui*
*Venture Business Laboratory, Hiroshima University, Higashi-Hiroshima, 739-8527, Japan*

Norio Ogita and Masayuki Udagawa
*Faculty of Integrated Arts and Sciences, Hiroshima University, Higashi-Hiroshima, 739-8521, Japan*

Masami Tsubota and Fumitoshi Iga
*Department of Quantum Matter, ADSM, Hiroshima University, Higashi-Hiroshima, 739-8530, Japan*

(Received 3 May 2003; published 14 January 2004)

Raman scattering spectra of single crystalline $Y_{1-x}Ca_xTiO_3$ ($x=0$, 0.10, 0.30, 0.37, 0.38, and 0.41) have been systematically studied in the temperature region from 298 to 8 K. The structural transition from the orthorhombic phase to the monoclinic one occurs below 200 K in $x \leqslant 0.38$. The intensity increase, related to the metal-insulator transition, has been observed below 100 K in $Y_{0.62}Ca_{0.38}TiO_3$. The phase separation from the monoclinic phase to the metallic orthorhombic and insulating monoclinic phase occurs below the metal-insulator transition temperature ($T_{MI}$) in $Y_{0.62}Ca_{0.38}TiO_3$. The intensity-increase is explained by the appearance of the orthorhombic structure below $T_{MI}$ and its anisotropic appearance is related to the random orientation of the principle axes of the orthorhombic grain.

DOI: 10.1103/PhysRevB.69.024102 PACS number(s): 78.30.−j, 71.30.+h, 64.70.Nd, 72.80.Ga

## I. INTRODUCTION

Perovskite-type transition-metal oxides with strong Coulomb interactions have recently attracted much interest because of their characteristic electronic and magnetic properties caused by a interplay of charge, spin, and orbital degrees of freedom.[1] $YTiO_3$ is well known as a Mott insulator showing a ferromagnetic transition at $T_c \sim 30$ K with a $3d^1$ (Ti) configuration and has a $GdFeO_3$-type structure with *Pbnm* symmetry at room temperature.[2,3] In $Y_{1-x}Ca_xTiO_3$, the insulator to metal transition occurs at $x \sim 0.38$.[2] In particularly, a temperature-induced metal-insulator (MI) transition has been clearly observed at around 130 K in $Y_{0.61}Ca_{0.39}TiO_3$.[4]

Recent powder x-ray diffraction experiments at around $x=0.39$ have reported that the structural phase transition from orthorhombic [$Pbnm(D_{2h}^{16})$] to monoclinic [$P2_1/n(C_{2h}^5)$] at around 230 K and also the phase separation between the low-temperature orthorhombic and monoclinic ones below the MI transition temperature ($T_{MI}$).[5] Raman scattering spectra of polycrystalline $Y_{1-x}Ca_xTiO_3$ at 50 K were reported by Katsufuji and Tokura,[6] but they did not discuss the correlations between the MI transition and the structural phase transition. Raman scattering is one of powerful tools to investigate lattice dynamics, including phonon anomalies related to the magnetic ordering or electron-lattice interactions. It has been applied to the orthorhombically distorted perovskite-type transition-metal oxides.[7–10]

In this paper, we have systematically studied the polarization and temperature dependence of Raman scattering spectra using single crystalline $Y_{1-x}Ca_xTiO_3$ in order to clarify the MI transition and the structural anomaly from a viewpoint of phonon dynamics. Part of the present study has already been reported in Ref. 11, where the phase separation from the monoclinic phase to the monoclinic+orthorhombic one occurs below $T_{MI}$ in $Y_{0.62}Ca_{0.38}TiO_3$. Here, we have studied in more detail the Ca-concentration dependence.

## II. EXPERIMENT

The single crystals of $Y_{1-x}Ca_xTiO_3$ were synthesized by a floating-zone method using an image furnace with halogen lamps under a reactive atmosphere of Ar and $H_2$ mixture. Details of sample preparation were reported in Ref. 12. In this experiment, the specimens with $x=0$, 0.10, 0.30, 0.37, 0.38, and 0.41 were used. The sample surface was polished to avoid the diffused reflection of the incident light. Electrical resistivity was checked by a four-terminal method from 300 K down to 4.2 K. $T_{MI}$ of our sample at $x=0.38$ is about 120 K.

In the Raman scattering measurements, an $Ar^+$ laser light with a wavelength of 514.5 nm was employed as the incident beam. The scattered light was analyzed by a triple monochromator (JASCO, NR-1800), and the analyzed light was detected by a CCD multichannel detector (Princeton Instruments, LN/CCD-1100-PB).

In the orthorhombic structure of *Pbnm*, the number of the Raman active phonons ($\Gamma_O$) is given as $\Gamma_O = 7A_g + 7B_{1g} + 5B_{2g} + 5B_{3g}$.[7] Raman active phonons with total symmetry $A_g$ appear in the polarization geometries of (*a*,*a*), (*b*,*b*), and (*c*,*c*), while $B_{1g}$, $B_{2g}$, and $B_{3g}$ appear in (*a*,*b*), (*a*,*c*), and (*b*,*c*), respectively, where *a*, *b*, and *c* correspond to the [1,0,0], [0,1,0], and [0,0,1] axes of the orthorhombic structure. In the symbol of $k_i(p_i,p_s)k_s$, *k* and *p* are the directions of the propagation and polarization of light, respectively, and the suffix of *i* and *s* denote the incident and scattered light, respectively.

## III. RESULTS

### A. Raman scattering of $YTiO_3$

The polarization dependence at room temperature and 8 K for $YTiO_3$ are shown in Figs. 1(a) and 1(b), respectively. The

 

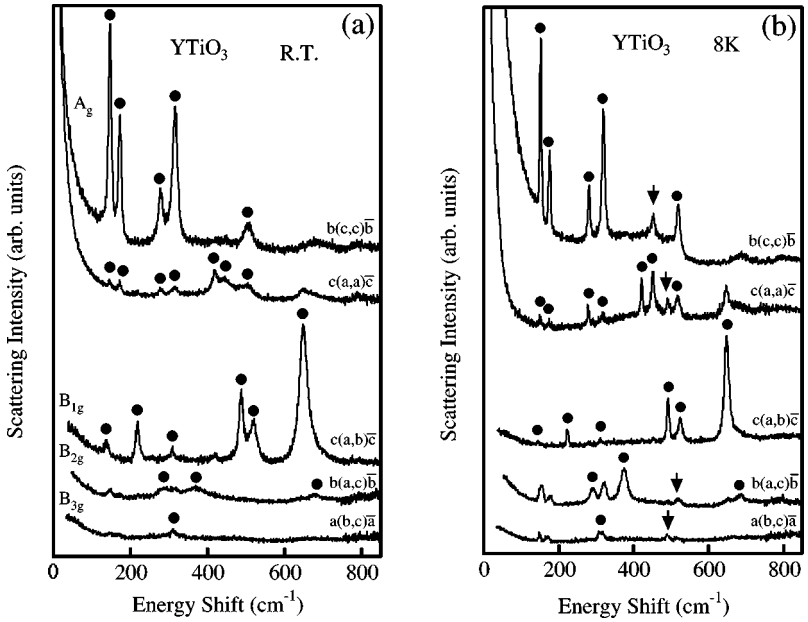


FIG. 1. Polarization dependence at (a) room temperature and (b) 8 K for $YTiO_3$. Closed circles denote the assigned phonons by *Pbnm* and the arrow is the additional phonon observed below 200 K.

peaks below 700 $cm^{-1}$ have been assigned as phonons. The assigned phonons by the symmetry of *Pbnm* are marked by the closed circles in Fig. 1(a). At room temperature, their observed number satisfies this symmetry.

However, new additional phonons, marked by the arrows in Fig. 1(b), have been observed in (*a*,*a*), (*c*,*c*), (*a*,*c*), and (*b*,*c*) at 8 K. The crystal symmetry is not orthorhombic at 8 K, since the observed number of $A_g$ at 8 K exceeds the estimated number for *Pbnm*.

For the monoclinic symmetry of $P2_1/n$, the number of the Raman active phonons ($\Gamma_m$) is estimated as $\Gamma_m = 12A_g + 12B_g$. The structural transition from the orthorhombic to monoclinic one gives three possible structures in the monoclinic phase, since only one angle between the principle axes for the orthorhombic phase deviates from right angle. In $YTiO_3$, our preliminary x-ray measurement reveals that the angle of $\alpha$ (angle between the *b* and *c* axes) changes from the right angle below 200 K. Thus, in this monoclinic structure, the $A_g$ modes appear in the polarization geometries of (*a*,*a*), (*b*,*b*), (*c*,*c*), (*b*,*c*), and $B_g$ in (*a*,*b*) and (*a*,*c*). The observed number of phonon modes below 200 K is well explained by the $P2_1/n$ symmetry. The wave numbers of the assigned phonons by the symmetry of *Pbnm* at room temperature and $P2_1/n$ at 8 K are summarized in Table I.

Temperature dependence of the integrated intensities of the new peaks, marked by the arrows in Fig. 1(b), is shown in Fig. 2. The peak intensities increase with decreasing temperature below 200 K. Thus, this result shows that the structural phase transition from orthorhombic to monoclinic one occurs below 200 K in $YTiO_3$.

### B. Raman scattering of Ca-doped crystals

The results of the Ca-concentration dependence at room temperature are shown in Fig. 3(a), where the $c(a,a)\bar{c}$ spectra are presented as the representative result. In Fig. 3(b), the peak energies, depicted by the closed circles in Fig. 3(a), are plotted against the Ca concentration. The *x* dependence of the observed phonon energy gradually changes. In the mixed crystal, according to Chang and Mitra,[13] there are two types of phonons: ''one mode'' and ''two mode.'' In the one-mode type, the phonon energy gradually changes from one end energy to the other end energy, while there are two peaks with each end energy in the intermediate concentration for the two-mode type. The present observed phonons are recognized as the one-mode type. The linewidths increase with increasing Ca-concentration for all observed phonon modes. At room temperature, all observed peaks are well assigned as

TABLE I. The assigned phonons by the symmetry of *Pbnm* at room temperature and $P2_1/n$ at 8 K. The accuracy of the energies is $\pm 1$ $cm^{-1}$ for sharp/strong peaks and $\pm 3$ $cm^{-1}$ for broad/weak peaks. The underline denotes the new peaks observed in $P2_1/n$.

| Mode | *Pbnm* at room temperature | Mode | $P2_1/n$ at 8 K |
|---|---|---|---|
| $A_g$ | 142 | $A_g$ | 147 |
| $A_g$ | 169 | $A_g$ | 171 |
| $A_g$ | 275 | $A_g$ | 276 |
| $A_g$ | 311 | $A_g$ | 306 |
| $A_g$ | 416 | $A_g$ | 316 |
| $A_g$ | 440 | $A_g$ | 419 |
| $A_g$ | 500 | $\underline{A_g}$ | $\underline{449}$ |
| $B_{1g}$ | 134 | $\underline{A_g}$ | $\underline{489}$ |
| $B_{1g}$ | 215 | $\underline{A_g}$ | $\underline{515}$ |
| $B_{1g}$ | 305 | $A_g$ | 670 |
| $B_{1g}$ | 483 | $B_g$ | 143 |
| $B_{1g}$ | 513 | $B_g$ | 221 |
| $B_{1g}$ | 646 | $B_g$ | 290 |
| $B_{2g}$ | 290 | $B_g$ | 309 |
| $B_{2g}$ | 365 | $B_g$ | 372 |
| $B_{2g}$ | 676 | $B_g$ | 490 |
| $B_{3g}$ | 305 | $\underline{B_g}$ | $\underline{517}$ |
| | | $\underline{B_g}$ | $\underline{646}$ |
| | | $B_g$ | 683 |

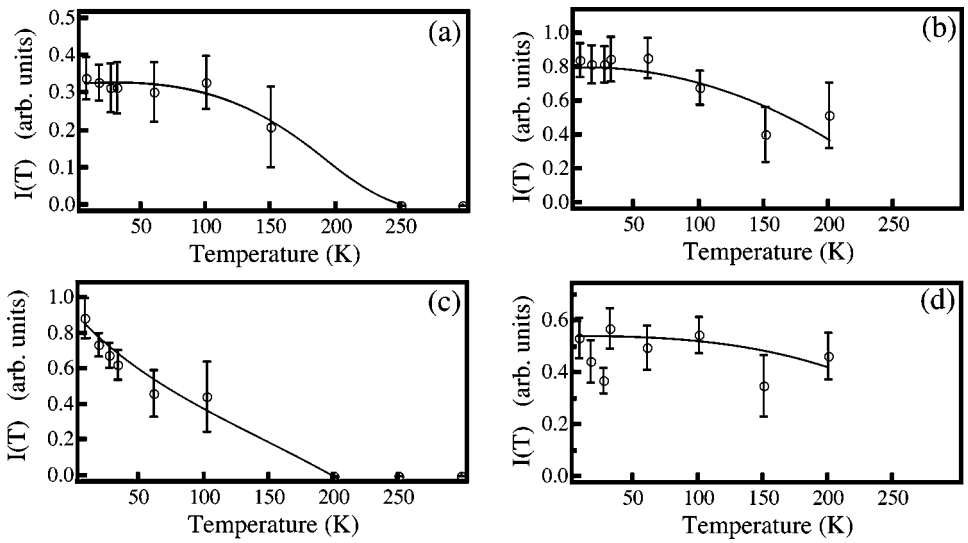


FIG. 2. Temperature dependence of integrated intensity, $I(T)$, at about (a) 490 $cm^{-1}$ in $c(a,a)\bar{c}$, (b) 445 $cm^{-1}$ in $b(c,c)\bar{b}$, (c) 515 $cm^{-1}$ in $b(a,c)\bar{b}$ and (d) 490 $cm^{-1}$ in $a(b,c)\bar{a}$ for $YTiO_3$. Solid lines are drawn as a guide to the eye.

the phonons with the symmetry of *Pbnm*, since the number of the observed peaks satisfies this symmetry for $x \leqslant 0.41$.

The samples with $x=0.37$ and 0.38 show maximum resistivities around 60 and 120 K, respectively, while $x=0.41$ sample shows metallic behavior from 300 to 1.5 K.[5] The MI transition is clearly observed for the $x=0.38$ sample at 120 K, since the resistivity decreases with decreasing temperature below 120 K. For the $x=0.37$ sample, the transition is not so clear, because the metallic behavior has not been observed even at 12 K.[5]

The polarization dependence at 12 K for $x=0.37$, 0.38, and 0.41 is summarized in Fig. 4. The spectral shapes of $x=0.37$ are quite different from those of $x=0.38$ and 0.41 at 12 K, while those of $x=0.38$ and 0.41 are similar, except for $c(a,a)\bar{c}$. The main difference is the observation of the strong peaks marked by $P_1$ and $P_2$.

For $x=0.38$, polarization dependence of $P_1$ and $P_2$ is anomalous at 12 K, since they have not been observed for $c(a,a)\bar{c}$, which is quite different from $b(a,a)\bar{b}$ and is similar to $c(a,a)\bar{c}$ for $x=0.37$. This result indicates that the spectra strongly depend on the propagation direction and are highly anisotropic for $x=0.38$. We note that $P_1$ and $P_2$ are not new peaks due to the MI transition, but the increase of the intensity of $P_1$ and $P_2$ is related to the transition, since they exist even at room temperature with the very weak intensity.

To understand the correlation between the intensity-increase of $P_1$ or $P_2$ and the MI transition, the temperature dependence of $b(c,c)\bar{b}$ is shown in Fig. 5 as the representative result. The spectra at room temperature are very similar. At low temperatures, the intensity of $P_1$ and $P_2$ dramatically develops below 120 K for $x=0.38$, but the spectra of $x=0.37$ and 0.41 change gradually.

The intensity increase of $P_1$ and $P_2$ for $x=0.38$ is not simple, as shown in Fig. 6, where the temperature depen-

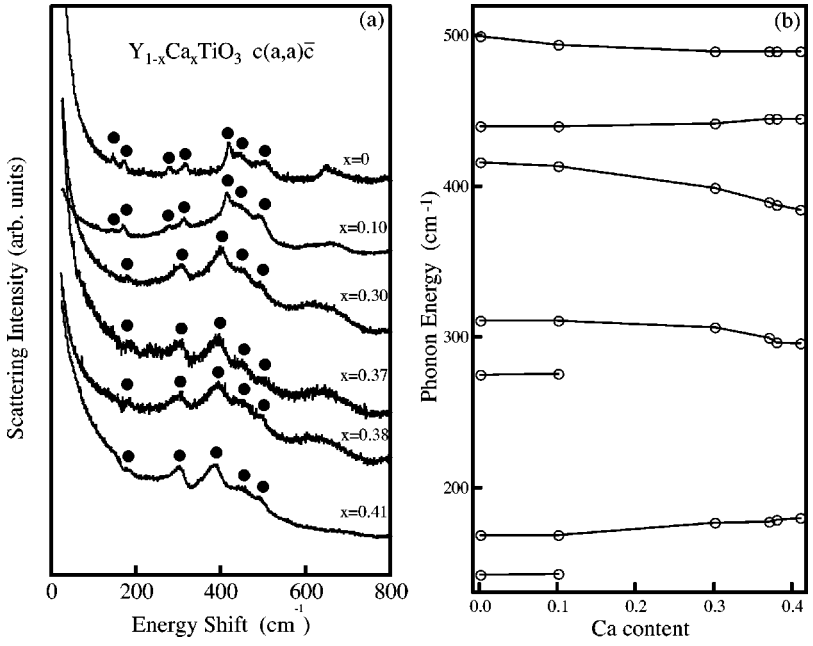


FIG. 3. Ca-concentration dependence of (a) $c(a,a)\bar{c}$ and (b) phonon energy in $c(a,a)\bar{c}$ at room temperature for $Y_{1-x}Ca_xTiO_3$, with $x=0$, 0.10, 0.30, 0.37, 0.38, and 0.41. Closed circles denote the assigned phonons by *Pbnm*.

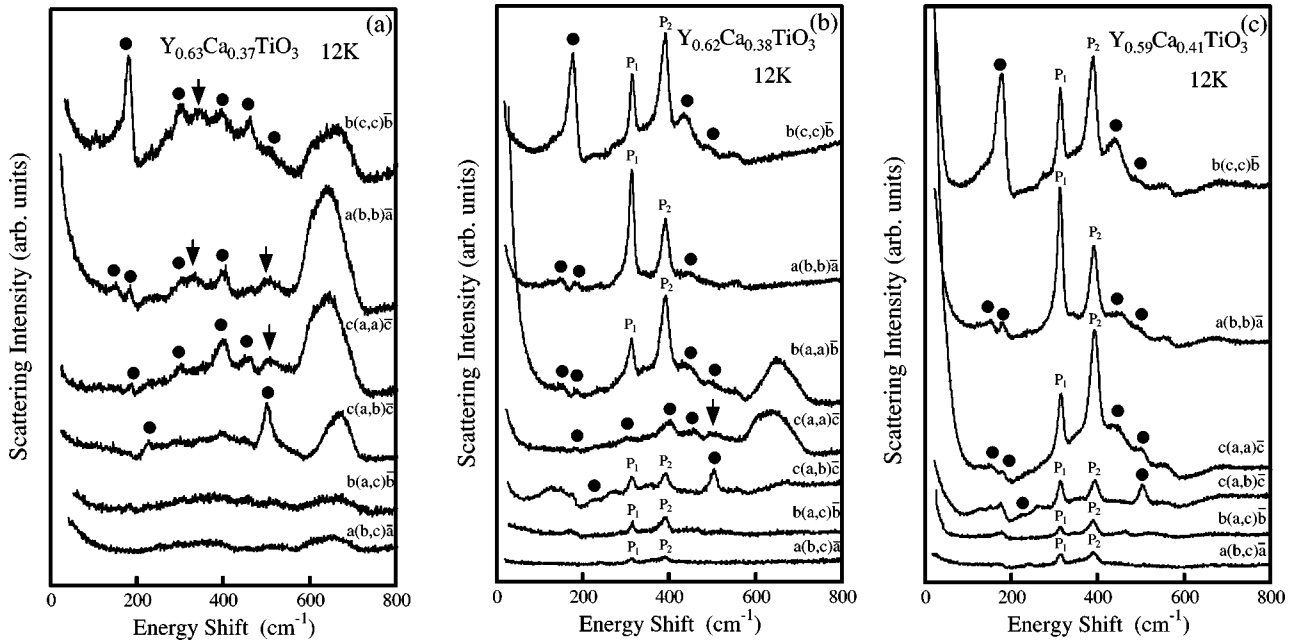


FIG. 4. Polarization dependence at 12 K for (a) $Y_{0.63}Ca_{0.37}TiO_3$, (b) $Y_{0.62}Ca_{0.38}TiO_3$, and (c) $Y_{0.59}Ca_{0.41}TiO_3$. Closed circles denote the assigned phonons by *Pbnm* at room temperature and the arrows are the additional phonons observed below 200 K. Remarkable peaks are marked by $P_1$ or $P_2$.

dence of $a(b,b)\bar{a}$ is presented. In this geometry, the intensity-increase of $P_1$ and $P_2$ occurs at 12 K with the decrease of temperature, and the intensity decreases at ~120 K with increasing temperature as shown in the bottom spectra of Fig. 6(a). In $c(a,a)\bar{c}$ the intensity development has not been observed down to 12 K, as shown in Fig. 4(b). Therefore, the intensity development of $P_1$ and $P_2$ strongly depends on the polarization geometries for $x=0.38$. On the other hand, for $x=0.41$, the intensity development of $P_1$ and $P_2$ is continuous from room temperature to low temperatures, as shown in Figs. 5(c) and 6(b). Here we note that $P_1$ and $P_2$ correspond to the peaks observed by Katsufuji and Tokura.[6]

According to the x-ray results,[5] the sample at about $x=0.39$ has two phases with orthorhombic and monoclinic ones below $T_{MI}$. Thus, it must be determined which phase is related to the increase of the intensity of $P_1$ and $P_2$. Before this determination, we describe the structural phase transition from orthorhombic to monoclinic one at about 200 K. As described in $YTiO_3$, the existence of the monoclinic phase is judged by the appearance of new additional peaks below 200 K. The additional peaks are marked by the arrows in Figs. 4, 5, and 6. The energies of the additional peaks are similar with these for $YTiO_3$. Thus, the observation of the additional peaks corresponds to the experimental evidence of the monoclinic symmetry.

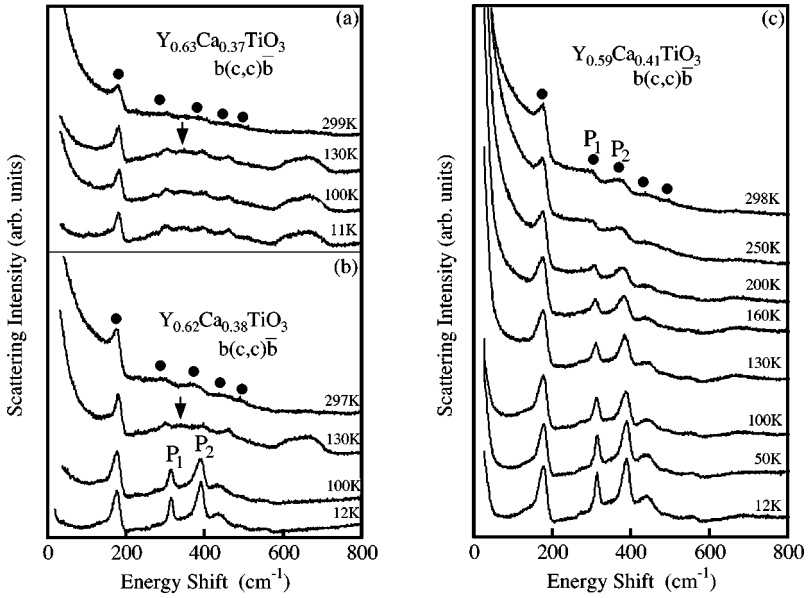


FIG. 5. Temperature dependence of $b(c,c)\bar{b}$ for (a) $Y_{0.63}Ca_{0.37}TiO_3$, (b) $Y_{0.62}Ca_{0.38}TiO_3$, and (c) $Y_{0.59}Ca_{0.41}TiO_3$. Note that $T_{MI}$ of $x=0.38$ is ~120 K. Closed circles denote the assigned phonons by *Pbnm* and the arrows are the additional phonons observed below 200 K. Remarkable peaks are marked by $P_1$ or $P_2$.

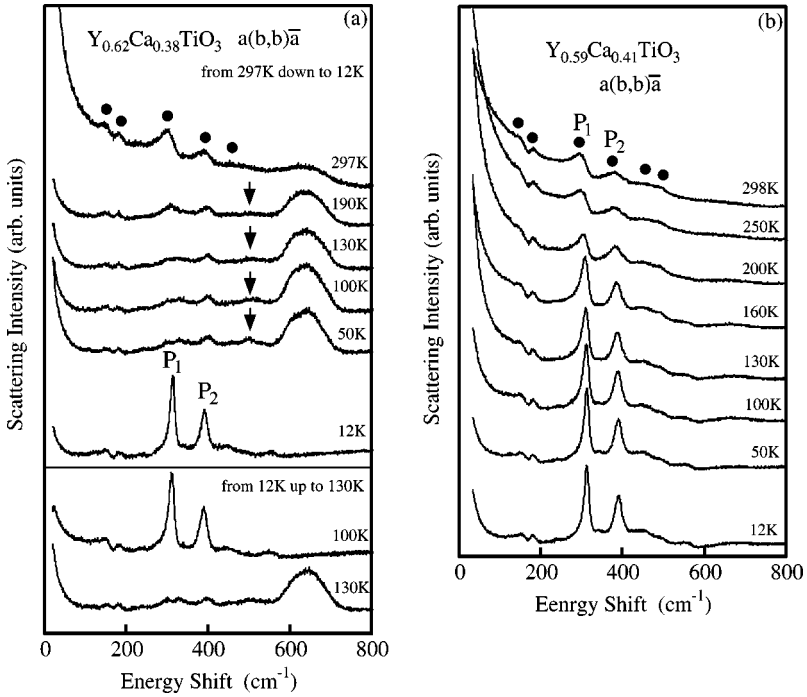


FIG. 6. Temperature dependence of $a(b,b)\bar{a}$ for (a) $Y_{0.62}Ca_{0.38}TiO_3$ and (b) $Y_{0.59}Ca_{0.41}TiO_3$. Closed circles denote the assigned phonons by *Pbnm* and the arrow is the additional phonon observed below 200 K. Remarkable peaks are marked by $P_1$ or $P_2$.

For $x=0.37$, as shown in Figs. 4(a) and 5(a), the additional peaks exist down to 11 K and the remarkable change of the peak intensity has not been observed. Thus, the dominant phase at low temperature is monoclinic for $x=0.37$. On the other hand, for $x=0.41$, such new additional peaks related to the monoclinic phase have not been observed as shown in Figs. 4(c), 5(c), and 6(b). Then, the structure of $x=0.41$ is orthorhombic from room temperature to 12 K, and the intensities of $P_1$ and $P_2$ gradually increase with decreasing temperature.

For $x=0.38$, the situation is complicated, compared with the cases of $x=0.37$ and 0.41. The structural transition to the monoclinic phase occurs below 200 K, as shown in Figs. 4(b), 5(b), and 6(a), because the new additional peaks marked by arrows are observed. However, once the intensities of $P_1$ and $P_2$ increase with decreasing temperature, the new additional peaks disappear. Thus, based on the results of $x=0.37$ and 0.41, it can be concluded that the intensity increases of $P_1$ and $P_2$ are originated from the appearance of the orthorhombic structure.

The anomalous property of $x=0.38$ is also found in the temperature dependence of the energy of $P_1$ and $P_2$. The result is shown in Fig. 7, where the result of $a(b,b)\bar{a}$ is presented as the representative result. The temperature dependence is remarkably different between $x=0.37$ and 0.41. For $x=0.38$, with decreasing temperature from room temperature, the peak energies follow the line of $x=0.37$ and jump to that of $x=0.41$ at 12 K. In the increasing process from 12 K, they follow the line for $x=0.41$ and jump to that of $x=0.37$ at around 120 K. This energy jump from the line of $x=0.37$ to that of $x=0.41$ has been observed for all observed $P_1$ and $P_2$ for $x=0.38$. This result clearly shows that the intensity-increased $P_1$ and $P_2$ is caused by the appearance of the orthorhombic structure. Thus, $P_1$ and $P_2$ are assigned as the phonons in the *Pbnm* symmetry. The assigned phonons by *Pbnm* at 12 K in $a(b,b)\bar{a}$ for $x=0.38$ and $x=0.41$ are summarized in Table II.

As other experimental result related to the MI transition, we can point out the broad peak at $\sim$ 650 cm$^{-1}$. For $x=0.37$, the intensity of this peak gradually increases with decreasing temperature as shown in Fig. 5(a) and this peak is observed for all polarization geometries at 12 K [Fig. 4(a)]. For $x=0.41$, the intensity of this peak does not develop with the decrease of temperature [Figs. 5(c) and 6(b)] and is very weak at 12 K [Fig. 4(c)]. However, for $x=0.38$, the peak disappear as shown in Figs. 5(b) and 6(a), when the intensities of $P_1$ and $P_2$ dramatically increase. This correlation is very similar to that for the additional peaks due to the monoclinic phase. At this stage, this peak has not been assigned as phonons because of the too broad linewidth.

We summarize the experimental results related to MI-transition observed by Raman scattering in Table III, where the intensity-increased temperature of $P_1$ and $P_2$ ($T_A$) and disappearance of the monoclinic and 650 cm$^{-1}$ peaks are listed for all polarization geometries.

### C. Low-energy excitation

In $YTiO_3$, no remarkable change between 300 and 8 K has been observed in the low-energy region below 200 cm$^{-1}$ as shown in Figs. 1(a) and 1(b). However, for $x=0.37$, 0.38, and 0.41, the change of the spectral shape and the intensity decrease below 200 cm$^{-1}$ have been found with decreasing temperature, as shown in Figs. 5, 6, and 8. In Fig. 8, the temperature dependence of $c(a,b)\bar{c}$ is shown for $Y_{0.63}Ca_{0.37}TiO_3$ and $Y_{0.59}Ca_{0.41}TiO_3$. Furthermore, the dip-like spectra have been observed at 200 cm$^{-1}$ for $x\geqslant 0.37$ at 12 K and become clear for the higher conductive samples. This low-energy response cannot be explained by the phonons. It might be originated from the electronic or mag-

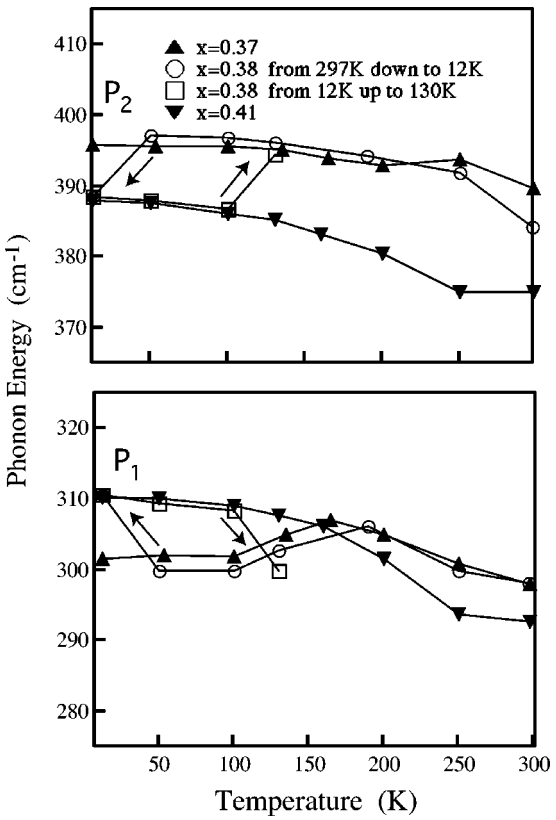


FIG. 7. Temperature dependence of phonon energies of $P_1$ and $P_2$ in $a(b,b)\bar{a}$ for $Y_{0.62}Ca_{0.38}TiO_3$ from 297 K down to 12 K and from 12 K up to 130 K. Temperature dependence of the phonon energies for $Y_{0.63}Ca_{0.37}TiO_3$ and $Y_{0.59}Ca_{0.41}TiO_3$ from room temperature to 12 K are also shown for comparison.

TABLE II. The assigned phonons ($cm^{-1}$) by the symmetry of *Pbnm* at 12 K in $a(b,b)\bar{a}$ for $x=0.38$ and 0.41 samples. Measurement accuracy $\pm 1$ $cm^{-1}$ for sharp/strong peaks and $\pm 5$ $cm^{-1}$ for broad/weak peaks.

| Mode | $x=0.38$ | $x=0.41$ |
|---|---|---|
| $A_g(1)$ | 148 | 149 |
| $A_g(2)$ | 181 | 179 |
| $A_g(4)$ | 311 | 310 |
| $A_g(5)$ | 389 | 388 |
| $A_g(6)$ | 445 | 443 |
| $A_g(7)$ | | 495 |

netic excitation. Thus, the anomalous low-energy spectra are probably due to the electronic excitation, judging from no magnetic fluctuation for $x \geqslant 0.37$. The further line-shape analysis for the low-energy excitations has not been proceeded, since the electronic density of state is unclear at this stage.

## IV. DISCUSSION

From the present experiments, the following results are clarified for $Y_{1-x}Ca_xTiO_3$ in relation to the MI transition. The peaks of $P_1$ and $P_2$ in $x=0.38$ show a drastic intensity increase below $T_{MI}$ and are the phonons with the orthorhombic symmetry. However, the mechanism of this property is not clear, since the intensity-increase of $P_1$ and $P_2$ is highly anisotropic and has the large temperature hysteresis as shown in Fig. 6(a). We discuss these unclear properties and remaining problems.

TABLE III. Qualitative comparison of the temperature dependence of the peak intensity at around $T_{MI}$ in the decreasing process in $Y_{0.62}Ca_{0.38}TiO_3$ and $Y_{0.59}Ca_{0.41}TiO_3$. The observed temperatures of drastic increase of $P_1$ and $P_2$ ($T_A$) are written in the table. The peak at about 340 or 500 $cm^{-1}$ is the peak observed below 200 K and correspond to the structural phase transition from the orthorhombic to the monoclinic phase, as shown by the arrow in Figs. 5(a), 5(b), and 6(a). In $b(a,a)\bar{b}$, the peak cannot be separated the monoclinic one from the $A_g(7)$ mode at $x=0.38$, as shown Fig. 4(b). We note that measurements were performed in the same sample at $x=0.38$ and 0.41, respectively.

| $x$ | polarization geometry | $P_1$ and $P_2$ | monoclinic peak | broad peak at 650 $cm^{-1}$ |
|---|---|---|---|---|
| 0.38 | $b(a,a)\bar{b}$ | continuous increase | remain | remain |
| | $c(a,a)\bar{c}$ | not observed | remain | remain |
| | $a(b,b)\bar{a}$ | 12 K | disappear | disappear |
| | $c(b,b)\bar{c}$ | 12 K | disappear | disappear |
| | $a(c,c)\bar{a}$ | 50 K | disappear | disappear |
| | $b(c,c)\bar{b}$ | 100 K | disappear | disappear |
| | $c(a,b)\bar{c}$ | 12 K | no peak | disappear |
| | $b(a,c)\bar{b}$ | 100 K | a little decrease | disappear |
| | $a(b,c)\bar{a}$ | 12 K | disappear | disappear |
| 0.41 | $c(a,a)\bar{c}$ | continuous increase ~200 K | no peak | a little peak |
| | $a(b,b)\bar{a}$ | continuous increase ~200 K | no peak | a little peak |
| | $b(c,c)\bar{b}$ | continuous increase ~200 K | no peak | a little peak |
| | $c(a,b)\bar{c}$ | continuous increase ~130 K | no peak | a little peak |
| | $b(a,c)\bar{b}$ | continuous increase ~130 K | no peak | a little peak |
| | $a(b,c)\bar{a}$ | continuous increase ~130 K | no peak | a little peak |

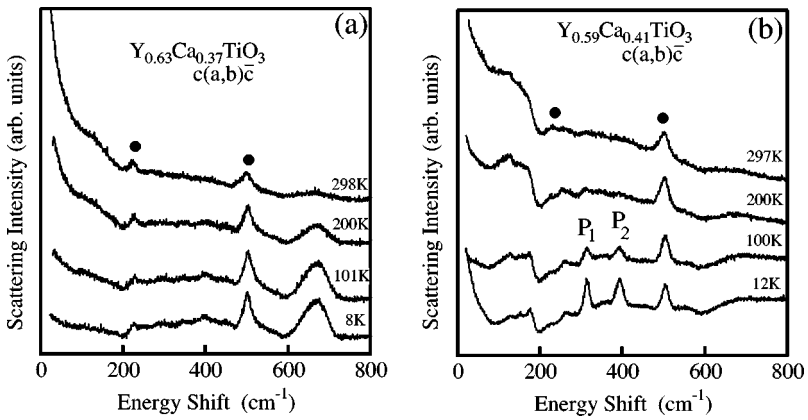


FIG. 8. Temperature dependence of $c(a,b)\bar{c}$ for (a) $Y_{0.63}Ca_{0.37}TiO_3$ and (b) $Y_{0.59}Ca_{0.41}TiO_3$. Closed circles denote the assigned phonons by *Pbnm*. Remarkable peaks are marked by $P_1$ or $P_2$.

The intensity-increase temperature of $P_1$ and $P_2$ is not systematic as shown in Table III. To clarify this, we have measured the anisotropy of resistivity of our sample used in the Raman scattering measurements by a four-terminal method. The results are shown in Fig. 9. In our sample, the resistivity along the *a* and *c* axes clearly show the MI transition around 120 K, but that along the *b* axis is similar to the reported results for $x=0.37$.[5] The results of the resistivity do not give us the plausible conclusion for the polarization dependence of the intensity-increased $P_1$ and $P_2$, since they are observed in most of the polarization geometries at 12 K in the polycrystalline sample. Thus, we cannot proceed the discussion based on the experimental evidences for this problem.

Next we discuss the effect of the monoclinic phase on the MI transition in the $Y_{1-x}Ca_xTiO_3$ system. According to Kato *et al.*, the resistivity of $x=0.41$ is metallic between room temperature and 1.5 K, and the volume fraction of the monoclinic phase is less than 40% in the same temperature region, while the MI transition occurs for the volume fraction of the monoclinic phase less than 50% for $x=0.39$.[5] It can be deduced from the above that the MI transition occurs for the volume fraction of the orthorhombic phase greater than 50%. Thus, the existence of the large volume fraction of the monoclinic phase changes the insulator, and the orthorhombic structure plays the important role for the MI transition at $x=0.38$. As the relation of this discussion, we note the reason of the abrupt intensity-increase of $P_1$ and $P_2$ below $T_{MI}$ at $x=0.38$. For $x=0.41$, the observed Raman spectra gradually change from room temperature to the low temperatures without any remarkable change. Thus, this result suggests that the intensity increase is caused by a switching from the monoclinic phase to the orthorhombic one, where the intensities of $P_1$ and $P_2$ are strong at the low temperature. Such switching is also observed in the energies of $P_1$ and $P_2$.

For $x=0.38$ and $x=0.41$, according to the x-ray experiments,[5] the monoclinic angle is $\beta$ (angle between *a* and *c* axes) below 200 K. The precise critical concentration of the monoclinic angle from $\alpha$ at $x=0$ to $\beta$ at $x\geqslant 0.37$ has not been reported. In this monoclinic structure with $\beta \neq 90°$, the $A_g$ modes appear in the polarization geometries of (*a*,*a*), (*b*,*b*), (*c*,*c*), and (*a*,*c*), and $B_g$ in (*a*,*b*) and (*b*,*c*) for $x=0.38$ and $x=0.41$. We emphasize that intensity increases of $P_1$ and $P_2$ are observed even in $c(a,b)\bar{c}$ and $a(b,c)\bar{a}$ [Figs. 4(b) and 4(c)] at 12 K, of which the symmetry is $B_g$ for monoclinic or $B_{1g}/B_{3g}$ for orthorhombic. Thus, this poor polarization dependence of $P_1$ and $P_2$ suggests the random orientation of the principle axes of the orthorhombic grains below $T_{MI}$ at $x=0.38$. This two-phase state reported by Kato *et al.*[5] is also observed by Raman scattering, since the monoclinic peak at about 500 $cm^{-1}$ exists even at 12 K below $T_{MI}$, as shown in Fig. 4(b).

At room temperature the polarization dependence satisfies the symmetry of *Pbnm*, but it is broken at low temperature even for $x=0.41$. The reported volume fraction of the monoclinic is 15% at 20 K. Thus, the orthorhombic structure at low temperature might be different from that at room temperature or be the complicated mosaic structure due to the two-phase coexistence. In the latter, the orthorhombic structure might be the same as that at room temperature. In order to understand this problem, the experimental determination of the size of each grain and the structure at the domain boundary is important by electron microscopy or scanning tunneling microscopy. These information will tell us the mechanism of the poor polarization dependence and the anisotropic appearances of $P_1$ and $P_2$.

The similar phase separation is reported in manganites. In this system, it has been recognized that MI transition is caused by the electronic phase separations into ferromagnetic

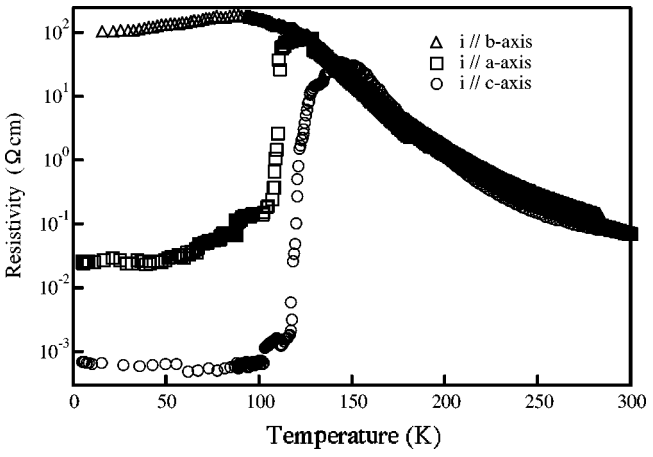


FIG. 9. Temperature dependence of electrical resistivity along the *a*, *b*, and *c* axes from room temperature down to 4.2 K for $Y_{0.62}Ca_{0.38}TiO_3$.

metallic domains and charge ordered insulating domains.[14–16] The size of domains is estimated on a length scales of 20–30 nm in $La_{0.5}Ca_{0.5}MnO_3$ by an electron microscopy.[15]

Finally, we summarize the remaining problems. A normal mode analysis is necessary to clarify the mechanism of the intensity-increase of $P_1$ and $P_2$. As described above, the measurements of the grain size by electron microscopy or scanning tunneling microscopy is the most important experiment to clarify the mechanism of the MI transition in $Y_{1-x}Ca_xTiO_3$.

## V. SUMMARY

We have systematically studied the Raman scattering spectra of single crystalline $Y_{1-x}Ca_xTiO_3$. The phase transition from the orthorhombic phase to the monoclinic one occurs below 200 K in $x \leqslant 0.38$. The phase separation from the monoclinic phase to the orthorhombic plus monoclinic phase occurs below the MI transition temperature in $Y_{0.62}Ca_{0.38}TiO_3$. Furthermore, the orthorhombic structure plays an important role for the MI transition at $x = 0.38$. The anisotropic observation of the intensity-increase is understood by the coexistence of the orthorhombic and monoclinic phases. An anomalous low-energy excitation from 0 to 200 $cm^{-1}$ has been observed for the conductive samples with $x \geqslant 0.37$.

## ACKNOWLEDGMENTS

This work was supported in part by a Grant-in-Aid for COE Research (No. 13CE2002) of the Ministry of Education, Culture, Sports, Science and Technology of Japan. The Raman scattering experiment was supported by the N-BARD of Hiroshima University.

*Email address: tsurui@imr.tohoku.ac.jp

[1] M. Imada, A. Fujimori, and Y. Tokura, Rev. Mod. Phys. **70**, 1039 (1998).
[2] Y. Taguchi, Y. Tokura, T. Arima, and F. Inaba, Phys. Rev. B **48**, 511 (1993).
[3] K. Kumagai, T. Suzuki, Y. Taguchi, Y. Okada, Y. Fujishima, and Y. Tokura, Phys. Rev. B **48**, 7636 (1993).
[4] F. Iga, T. Naka, T. Matsumoto, N. Shirakawa, K. Murata, and Y. Nishihara, Physica B **223–224**, 526 (1996).
[5] K. Kato, E. Nishibori, M. Takata, M. Sakata, T. Nakano, K. Uchihira, M. Tsubota, F. Iga, and T. Takabatake, J. Phys. Soc. Jpn. **71**, 2082 (2002).
[6] T. Katsufuji and Y. Tokura, Phys. Rev. B **50**, 2704 (1994).
[7] M. Udagawa, K. Kohn, K. Koshizuka, T. Tsushima, and K. Tsushima, Solid State Commun. **16**, 779 (1975).
[8] M. N. Iliev, M. V. Abrashev, H.-G. Lee, V. N. Popov, Y. Y. Sun, C. Thomsen, R. L. Meng, and C. W. Chu, Phys. Rev. B **57**, 2872 (1998).
[9] M. Zaghrioui, A. Bulou, P. Lacorre, and P. Laffez, Phys. Rev. B **64**, 081102(R) (2001).
[10] H. Kuroe, I. Habu, H. Kuwahara, and T. Sekine, Physica B **316–317**, 575 (2002).
[11] T. Tsurui, N. Ogita, M. Udagawa, M. Tsubota, K. Uchihira, and F. Iga, Physica B **329–333**, 833 (2003).
[12] M. Tsubota, F. Iga, T. Takabatake, N. Kikugawa, T. Suzuki, I. Ogura, H. Kawanaka, and H. Bando, Physica B **281–282**, 622 (2000).
[13] I. F. Chang and S. S. Mitra, Adv. Phys. **20**, 359 (1971).
[14] C. H. Chen and S-W. Cheong, Phys. Rev. Lett. **76**, 4042 (1996).
[15] S. Mori, C. H. Chen, and S-W. Cheong, Phys. Rev. Lett. **81**, 3972 (1998).
[16] M. Uehara, S. Mori, C. H. Chen, and S-W. Cheong, Nature (London) **399**, 560 (1999).